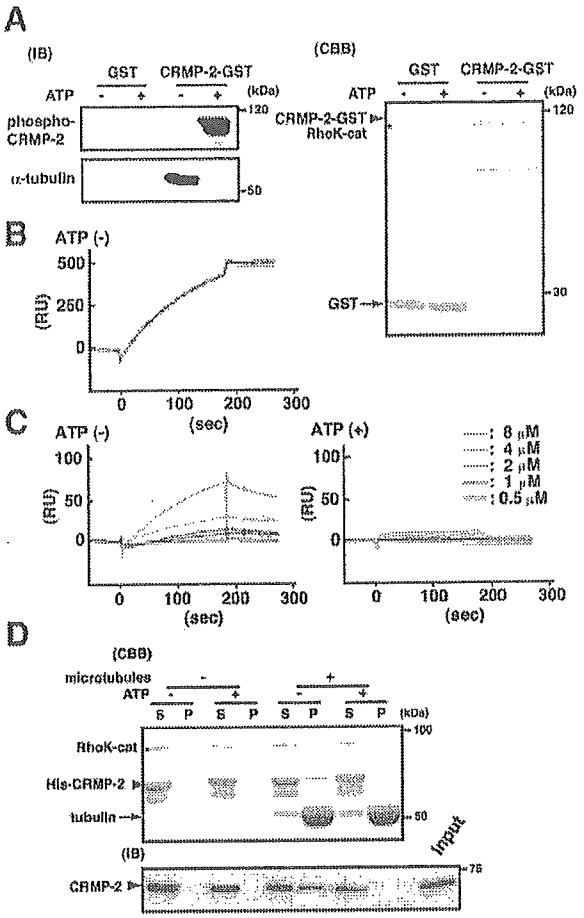

FIG. 1. An in vitro tubulin or microtubule binding assay using phosphorylated or nonphosphorylated CRMP-2-GST. (A) GST and CRMP-2-GST (0.5 μM) were phosphorylated by Rho kinase catalytic domain (RhoK-cat) in the presence (+) or absence (−) of ATP. GST or CRMP-2-GST immobilized onto beads was incubated with 1 μM tubulin in PEM buffer for 1 h at 4°C. GST and CRMP-2-GST results were shown with a Coomassie brilliant blue (CBB)-stained gel (right panel). Purified CRMP-2-GST contained degradation products, as confirmed by immunoblotting (IB) with anti-GST and anti-CRMP-2 antibody. An asterisk indicates RhoK-cat. An arrowhead and an arrow indicate the intact protein of CRMP-2-GST and GST, respectively. Phosphorylated CRMP-2-GST or the bound tubulin was analyzed by immunoblotting with anti-phospho-CRMP-2 antibody and anti-α-tubulin antibody (left panels). (B) Biacore sensorgram of tubulin capture with anti-tubulin antibody. Purified tubulin heterodimer (0.5 μM) was captured with the anti-α-tubulin antibody immobilized over the sensor chip at a flow rate of 10 μl/min for 3 min. The sensorgram in the sample of nonphosphorylated CRMP-2 [ATP (−)] is identical to that obtained with phosphorylated CRMP-2 [ATP (+)] (data not shown). The increase in RU (resonance units) results from the binding of tubulins to anti-tubulin antibodies. (C) Biacore sensorgram of CRMP-2 binding to tubulin. Binding of 8, 4, 2, 1, and 0.5 μM phosphorylated [ATP (+)] or nonphosphorylated [ATP (−)] His-CRMP-2 to a tubulin heterodimer-loaded sensor chip surface was examined. (D) Cosedimentation analysis of phospho-CRMP-2 or non-phospho-CRMP-2. His-CRMP-2 (5 μM) was phosphorylated by Rho kinase (RhoK-cat) in the presence (+) or absence (−) of ATP. His-CRMP-2 was mixed with 10 μM microtubules stabilized by Taxol (+) or left unmixed (−). After a 10-min incubation at 37°C, mixtures containing microtubules were centrifuged at 37°C. The quantity of His-CRMP-2 in supernatant (S) or pellet (P) was shown by Coomassie brilliant blue gel staining results (upper panel). The samples were analyzed by immunoblotting using anti-GST antibody to confirm the identity of this band as CRMP-2 (lower panel). An asterisk indicates RhoK-cat. An arrowhead and an arrow indicate His-CRMP-2 and tubulin, respectively.

calcium phosphate method with chick DRG neurons. The mean level of ectopic CRMP-2 expression is maximally fivefold that of the endogenous levels 3 days after transfection. For the analysis of axon length, we cultured DRG neurons without NGF. Spontaneous axon elongation was observed, probably because of the trophic factors secreted from contaminated neurotrophic cells or neurons.

Immunofluorescence study and microscopic observation. Vero cells, N1E-115 cells, and DRG neurons were fixed with 3.7% formaldehyde in phosphate-buffered saline (PBS) for 10 min at room temperature and then treated with 0.05% Triton X-100 for 10 min at 4°C. They were then treated with 1% BSA in PBS for 1 h at room temperature and incubated with the indicated antibodies. Immunoreactivity was visualized by incubation with fluorescein isothiocyanate (FITC)-conjugated anti-rabbit or mouse immunoglobulin antibodies (Amersham Biosciences Corp.) and Texas Red-conjugated anti-rabbit or mouse immunoglobulin antibodies (Amersham Biosciences Corp.). The images of immunostained cells or neurons were analyzed using a confocal laser microscopy system (LSM 510; Carl Zeiss, Oberkochen, Germany). Intensity of fluorescence was analyzed using the LSM 510 software.

For electron microscopic immunocytochemistry, DRG growth cones cultured on coverslips were fixed with 2% glutaraldehyde in 0.85 M cacodylate buffer adjusted to pH 7.4. Fixed samples were then dehydrated with an ascending series of ethanol up to 99.5% and embedded in Lowicryl K4M resin (Polysciences, Inc., Warrington, PA) according to the manufacturer's protocol. Immunolabeling was performed on the sections as described previously (50, 70).

For freeze-etching immunoreplica methods, growth cones cultured on large coverslips (13 × 13 mm) were washed once with PIPES buffer containing 10 mM PIPES, 100 mM KCl, 8 mM $MgCl_2$, and 3 mM EGTA. Small coverslips (5 × 5 mm) treated with alcian blue were placed on the growth cone-rich areas in a culture dish under the microscope. A fixative consisting of 1% glutaraldehyde and 2% paraformaldehyde in PIPES buffer was added immediately. Then coverslips were lifted slowly. In this way, apical plasma membranes of growth cones and axons were separated from the cytoplasm. After being washed with the buffer, isolated membranes attached to the coverslip were incubated with primary antibody raised against CRMP-2 or phosphorylated CRMP-2 in the PIPES buffer containing 1% BSA for 1 h. Samples were then labeled with 10 nm gold-conjugated secondary antibody (Amersham Biosciences Corp.) after being washed three times with the buffer for 1 h. After immunolabeling, specimens were rapidly frozen by plunging them onto a copper block cooled with liquid helium. Frozen specimens were brought into a freeze replica device (FR9000; Hitachi Science, Tokyo, Japan), slightly dried, and rotary shadowed with platinum and carbon. Shadowed specimens were removed from the coverslip in 5% hydrofluoric acid solution and observed under an electron microscope (1200 EX; JEOL Ltd., Tokyo, Japan).

Collapse assay. Both the transfected neurons and nontransfected neurons were cultured in serum plus medium for 20 h and then cultured in serum-free medium without NGF for 4 h. The collapse assay was performed as previously described (59). For the immunoblot analysis and the count of collapsed growth cones, neurons were stimulated with 1 μg/ml purified ephrin-A5-Fc. Although we know that the DRG neuron is not a common choice for studies of ephrin-A5, we used the same experimental system in a previous study employing Sema3A and lysophosphatidic acid (LPA) to obtain comparable results for ephrin-A5. It is reported that EphA2 and ephexin, a Rho nucleotide exchange factor, are expressed in DRG neurons (29, 61) and that DRG neurons react to ephrin-A5 and ephrin-A3 (19, 48). We observed better responses of ephrin-A5-stimulated DRG neurons in the absence of serum compared to those seen in the presence of serum. The pretreatment with 10 μM Rho kinase inhibitor (Y-27632 or HA1077) was performed for 1 h before the collapse assay. For immunoblot analysis, the cells were stimulated by ephrin-A5 for 3, 10, or 30 min at 37°C in serum-free medium without NGF. The cells were treated with 10% (wt/vol) trichloroacetic acid. The resulting precipitates were subjected to immunoblot analysis using anti-phospho-CRMP-2 and anti-CRMP-2 monoclonal antibody.

RESULTS

We previously showed that CRMP-2 binds to the tubulin dimer and enhances microtubule formation (28). We examined whether phosphorylation of CRMP-2 affects its tubulin binding

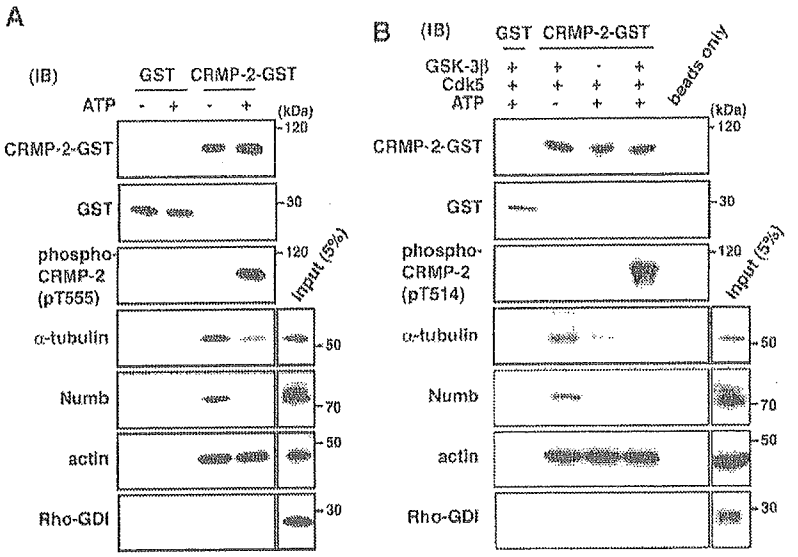

FIG. 2. An in vitro binding assay using phospho- or non-phospho-CRMP-2-GST and rat brain lysate. (A and B) GST and CRMP-2-GST (0.5 μM) were phosphorylated by Rho kinase catalytic domain (RhoK-cat) (A) or Cdk5 and/or GSK-3β (B) in the presence (+) or absence (−) of ATP. GST and CRMP-2-GST immobilized on beads were incubated with extracts of rat brain (P6 and P7) for 1 h at 4°C. CRMP-2-GST and the bound proteins were analyzed by immunoblotting (IB) using anti-GST antibody, anti-phospho-CRMP-2 antibody, anti-α-tubulin antibody, anti-Numb antibody, anti-Rho-GDI antibody, or anti-actin antibody. Input, immunoreactive bands of brain lysate (5% in total lysate). The lane labeled "beads only" shows the results for beads and brain lysates without GST proteins.

activity in vitro. Purified CRMP-2-GST was phosphorylated by RhoK-cat in the presence or absence of ATP. Phosphorylated CRMP-2 was detected by anti-phospho-CRMP-2 antibody, which specifically recognizes the phosphorylated state of CRMP-2 at Thr-555 (5) (Fig. 1A). Phosphorylated or nonphosphorylated CRMP-2 was immobilized on GST beads and incubated with purified tubulin heterodimer at 4°C. Tubulin was retained on the beads coated with nonphosphorylated CRMP-2, as reported previously (28), but not on the beads coated with phosphorylated CRMP-2 (Fig. 1A). The perturbation of the association of tubulin and CRMP-2 by phosphorylation was also confirmed by using the Biacore system (Fig. 1B and C). CRMP-2 bound to the retained tubulin in the Biacore sensor chip in a dose-dependent manner, whereas phosphorylated CRMP-2 did not (Fig. 1C). These results indicate that CRMP-2 phosphorylated by Rho kinase does not bind to the tubulin heterodimer.

We next examined whether phosphorylation of CRMP-2 affects its binding activity to microtubules in vitro (Fig. 1D) by use of a standard cosedimentation assay. Phosphorylated CRMP-2 or nonphosphorylated CRMP-2 was incubated with microtubules polymerized by Taxol at 37°C, and these mixtures were centrifuged to sediment the filamentous microtubules and the interacting molecules. BSA, a control protein, did not cosediment with microtubules (data not shown). Some nonphosphorylated CRMP-2 cosedimented with Taxol-stabilized microtubules, as reported previously (28). However, phosphorylated CRMP-2 was only minimally cosedimented. These results indicate that phosphorylation of CRMP-2 by Rho kinase decreases the ability of CRMP-2 to associate with microtubules as well as with tubulin heterodimers.

We next examined the effect of phosphorylation on the interaction of CRMP-2 with other molecules. We previously found that Numb binds to CRMP-2 directly and is localized at the axonal growth cone in neurons (56). The Numb and CRMP-2 complex mediates the endocytosis of L1 in the axonal growth cones, and Numb-mediated endocytosis of L1 is necessary for axon growth (56). We examined the interaction of phosphorylated CRMP-2 with partner proteins, including Numb, by a GST pulldown assay using rat brain lysate (Fig. 2A and B). Phosphorylated or nonphosphorylated CRMP-2 was immobilized on GST beads and incubated with postnatal rat brain lysate. An association of Numb with the beads coated with CRMP-2-GST was observed but not with the beads of phosphorylated CRMP-2-GST at Thr-555, suggesting that CRMP-2 phosphorylated by Rho kinase loses the ability to bind to Numb as well as tubulin (Fig. 2A). A small amount of tubulin was retained by phosphorylated CRMP-2 under these conditions, presumably because the high concentration of tubulin (approximately 13 μM) in brain lysates increased the efficiency of tubulin binding to phosphorylated CRMP-2 (Fig. 2A). Rho-GDI (a cytosolic and abundant protein used as a negative control) did not associate with CRMP-2. In addition, we identified actin as a CRMP-2-interacting molecule (Fig. 2A). Actin bound to phosphorylated CRMP-2 as well as to nonphosphorylated CRMP-2. These results indicate that CRMP-2 phosphorylation at the C terminus affects the interaction with certain proteins, including Numb and tubulin, but not with actin.

CRMP-2 can be phosphorylated by Cdk5 at Ser-522, and by recognizing this priming phosphorylation, GSK-3β phosphorylates CRMP-2 at Ser-518 and Thr-514 (10, 14, 68, 73). Since these phosphorylation sites are close to the phosphorylation site of Rho kinase, we examined whether these phosphorylations affect the association of CRMP-2 and interacting molecules. Similarly to Rho kinase results, the phosphorylation by

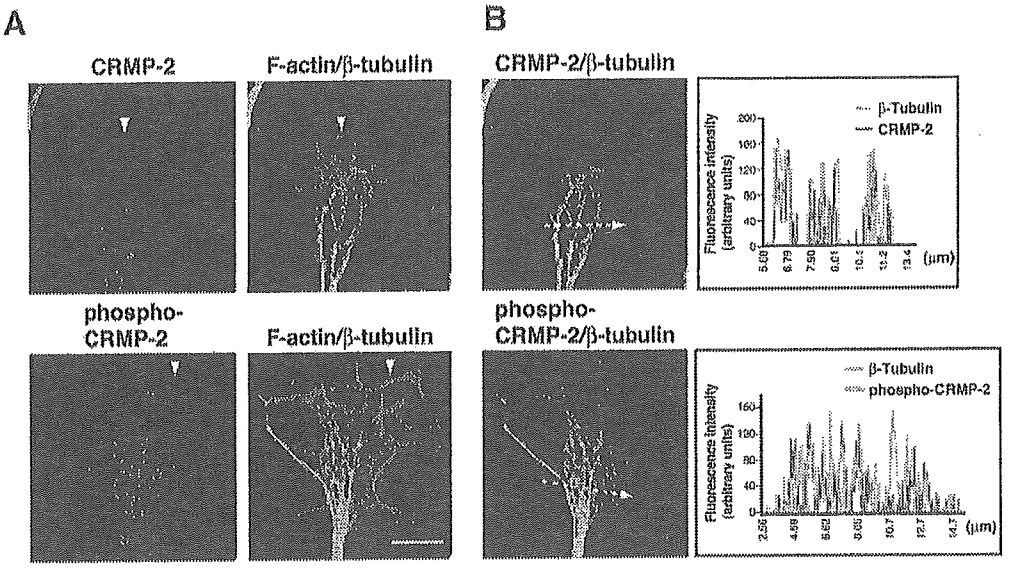

FIG. 3. Localization of CRMP-2 or phospho-CRMP-2 in chick DRG neuron growth cones. (A) Chick DRG neuron growth cones were triple stained with anti-CRMP-2 antibody (red), anti-unique β-tubulin antibody (green), and Alexa-649-phalloidin (blue) (upper panels) or anti-phospho-CRMP-2 antibody (red), anti-unique β-tubulin antibody (green), and Alexa-488-phalloidin (blue) (lower panels). Arrowheads indicate the colocalization of phosphorylated CRMP-2 or CRMP-2 and actin filaments. (B) Graphs plot the fluorescence intensity of immunolabeled CRMP-2 (red) and unique β-tubulin (green) or phosphorylated CRMP-2 (red) and unique β-tubulin (green) in the dotted line shown in each growth cone image. Bar, 10 μm.

Cdk5 and GSK-3β also prevents the binding of tubulin dimers and Numb but not that of actin (Fig. 2B). These results indicate that CRMP-2 phosphorylation at the C terminus by Rho kinase, Cdk5, and GSK-3β has similar effects on CRMP-2 function.

Next we examined the localization of CRMP-2 at DRG neuron growth cones. As reported previously, CRMP-2 is accumulated at the distal part of axons and growth cones (39, 54, 58). To examine the intracellular localization of phosphorylated CRMP-2 and interacting molecules, we performed an indirect immunofluorescence study using anti-phospho-CRMP-2 antibody (Fig. 3A). CRMP-2 immunoreactivity was mainly localized at the center of the growth cones and partially colocalized with microtubules and actin, as reported previously (56, 75). However, phosphorylated CRMP-2 was localized on punctate structures all around the growth cone area and some was seen even in the filopodia of the growth cones, which was stacked with actin filaments. Because phosphorylated CRMP-2 was present in all areas of growth cone, its immunoreactivity was overlapped with the filamentous image of microtubules. Localization of phosphorylated CRMP-2 itself did not appear to occur in the form of microtubule-like bundles or filaments, however, as was observed in experiments with anti-CRMP-2 antibody (Fig. 3B).

Subcellular localization of CRMP-2 in chick DRG growth cones was also examined by electron microscopic immunocytochemistry. As shown in immunofluorescence images (Fig. 3), microtubules were stuck and distributed in parallel. Immunolabeling in the electron micrograph was found predominantly on the filamentous image of microtubules but rarely in the background (Fig. 4A). In the grazing section of growth cones, the immunolabeling was also localized close to the edge, near the membranous areas, in addition to being localized at microtubules (Fig. 4B). This suggests that CRMP-2 is present in the vicinity of the plasma membrane of growth cones. For more-precise localization, we employed the freeze-etching immunoreplica method, which illustrates different morphological views, in particular, the membrane cytoskeletal complex (the so-called membrane undercoat). Freeze-etched images showed a few clathrin-coated pits and the cortical actin filaments in the cytoplasmic surface of the apical distal membrane (membrane undercoat) of growth cones. The high-power view of the cytoplasmic surface of the membrane provides evidence that CRMP-2 was localized on clathrin-coated pits (Fig. 4D and E) and actin filaments (Fig. 4G). More than 75% of the clathrin-coated pits showed immunolabeling of CRMP-2 (76.5%; n = 17). Because AP-2, which is a component of clathrin-coated pits, associates with Numb, CRMP-2 is thought to bind to clathrin-coated pits through Numb (56). In contrast, the immunolabeling against phosphorylated CRMP-2 was found only on actin filaments (Fig. 4H) and not on microtubules or clathrin-coated pits (0%, n = 15; Fig. 4C and F). These observations are morphological counterparts of the molecular interaction scheme derived from biochemical experiments on the basis of the idea that CRMP-2 associates with Numb on clathrin-coated pits, microtubules, or actin filaments, whereas phosphorylated CRMP-2 interacts only with actin filaments in growth cones.

We then examined the functional relevance of the relationship between phosphorylation at Thr-555 and CRMP-2 activity in neurons (Fig. 5A). We first characterized two CRMP-2 mutants, one in which the Rho kinase phosphorylation site (Thr-555) is replaced by Asp (CRMP-2 T555D), which is expected to mimic the phosphorylated form (3), and another in

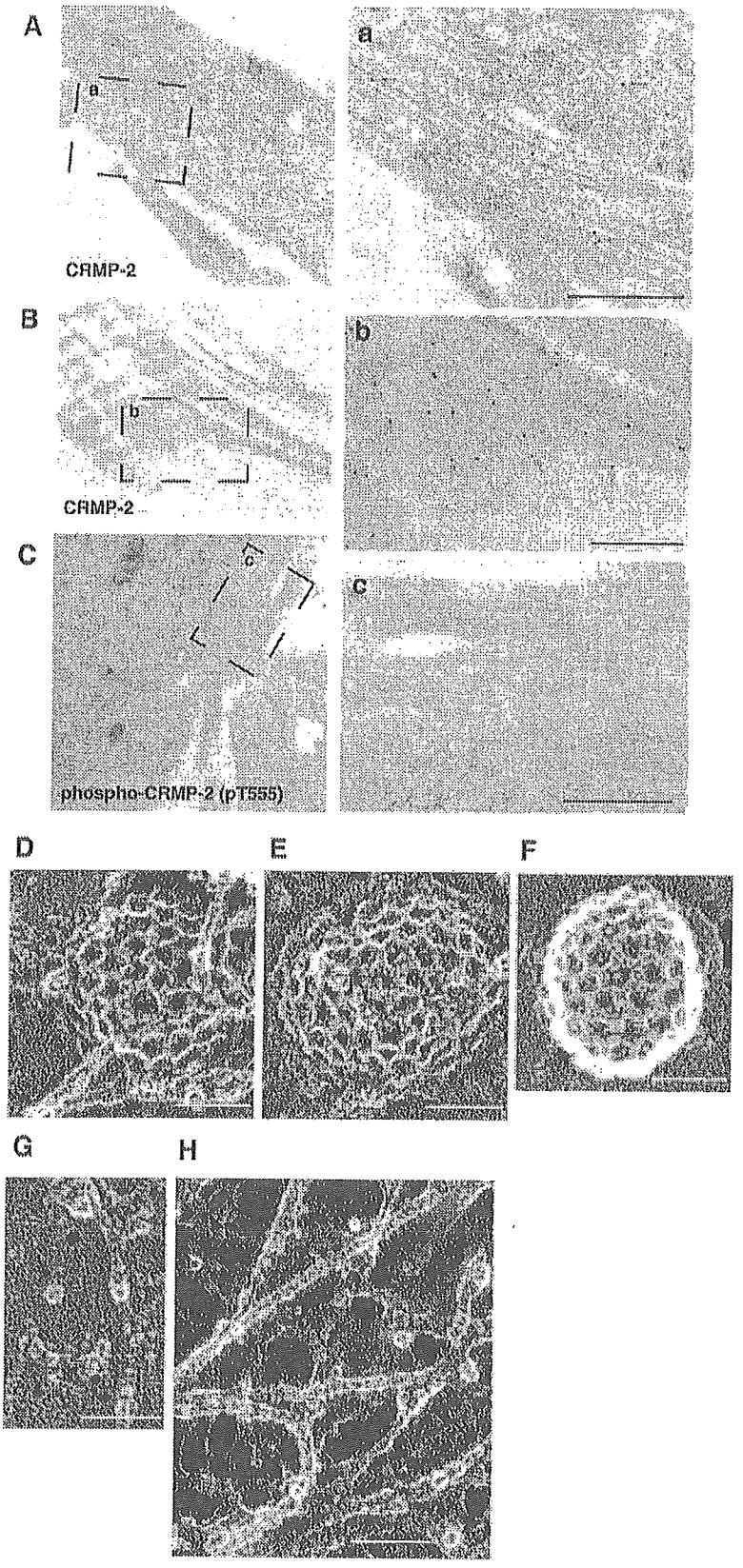
A
a
CRMP-2
B
b
CRMP-2
C
c
phospho-CRMP-2 (pT555)
D
E
F
G
H

which Thr-555 is replaced by Ala (CRMP-2 T555A) and is not phosphorylated by Rho kinase (5). Because ectopic green fluorescent protein (GFP)-tagged CRMP-2 was diffusely distributed, it was difficult to examine the localization of ectopic CRMP-2 in detail at the growth cones. Although we do not know why GFP mutants are located diffusely, this is presumably because neurons express CRMP-2 at levels much higher than other proteins (approximately 1% in total proteins). In contrast, in the cells expressing CRMP-2 at lower levels, we observed the clear colocalization of GFP-CRMP-2 and microtubules. When GFP-CRMP-2 wild type (WT) was expressed in Vero fibroblasts, 72.7% of GFP-tagged CRMP-2-expressing cells ($n = 22$) showed clear localization along the mitotic spindle, as previously described (28, 34) (Fig. 5A). Colocalization of the mutant CRMP-2 T555A with microtubules was also observed in 95.2% of the transfected cells ($n = 21$). However, the mutant CRMP-2 T555D was diffusely distributed, and only 9.5% of GFP-CRMP-2 T555D-expressing cells showed the colocalization with the mitotic spindle ($n = 21$).

Using these mutant constructs, we examined the functional relevance of phosphorylation at Thr-555 and CRMP-2 activity in terms of neurite formation (Fig. 5B). N1E-115 neuroblastoma cells were transfected with CRMP-2 T555D and CRMP-2 T555A. N1E-115 cells have a round morphology in the presence of serum, whereas these cells can differentiate and extend neurites in serum-free medium. In the presence of serum, only about 5% of the cells extended neurites. Under these conditions, expression of CRMP-2 WT increased the numbers of the cells bearing neurites, in contrast to the results seen with control cells expressing GST ($P < 0.01$), as described previously (28) (Fig. 5C). The expression of CRMP-2 T555A increased the percentage of cells bearing neurites ($P < 0.01$), but that of the T555D mutant only slightly increased the percentage ($P > 0.2$). This neurite formation in N1E-115 is known to require the assembly of the microtubules (28). The morphology of neurites induced by the ectopic expression of CRMP-2 WT or T555A was similar to that induced by the serum deprivation, and the neurites had microtubules that were detected with anti-α-tubulin antibody (28) (Fig. 5B).

We next examined the effects of these constructs on axon elongation in DRG neurons. Dissociated DRG neurons were transfected with the plasmids used in Fig. 5B. After transfection, neurons were cultured for 3 days in NGF-deprived medium. Under these conditions, some neurons transfected with control plasmids maintained the long axon. In neurons transfected with CRMP-2 WT, the percentage of the neurons bearing a long axon (>1,300 μm) was increased, in contrast to the control cells expressing GST ($P < 0.01$; Fig. 5D). CRMP-2 T555A had an effect on axon elongation similar to that seen with CRMP-2 WT ($P < 0.01$), but that of T555D was weak ($P < 0.05$). These observations indicate that the dephosphorylated form of CRMP-2 has the ability to promote axon elongation, presumably through the interaction with tubulin and Numb, and that the phosphorylated form of CRMP-2 loses most of ability to support neurite formation in N1E-115 and DRG neurons (Fig. 5C and D). Compared to control results, however, the mutant T555D has at least a weak ability to enhance neurite outgrowth or axon elongation (Fig. 5C and D). Although we do not know why T555D mutants have these positive effects on axon elongation, we think that the mutant T555D may not completely mimic the phosphorylated states, even though it increases the negative charge at the phosphorylation site, as previously reported (15, 25, 47). In fact, 9.5% of GFP-CRMP-2 T555D-expressing cells show the colocalization with mitotic spindles under the conditions in which 72.7% of GFP-CRMP-2 WT colocalized with spindles (Fig. 5A). Thus, it appears that the T555D mutant still keeps some activity to interact with tubulin and/or microtubules, thereby promoting neurite elongation. Alternatively, this implies the existence of other mechanisms that enhance neurite elongation, which are regulated independently of phosphorylation by Rho kinase at Thr-555.

As we reported previously, CRMP-2 is phosphorylated by Rho kinase during LPA-induced growth cone collapse (5). However, its physiological role in axon guidance is still unknown. Thus, we examined the physiological role of the phosphorylation of CRMP-2 by Rho kinase in growth cone collapse induced by repulsive guidance cues (Fig. 6). As some groups have reported, several repulsive axon guidance cues stimulate Rho/Rho kinase signaling to induce growth cone collapse (74). Among them, ephrin-A5 induces the phosphorylation of MLC through Rho kinase (71). We then examined whether ephrin-A5 induces CRMP-2 phosphorylation by Rho kinase at Thr-555. DRG neurons cultured for 24 h were serum starved for 4 h and then stimulated by ephrin-A5 for 3, 10, and 30 min; these stimuli induced growth cone collapse. The addition of ephrin-A5 induced rapid phosphorylation of endogenous CRMP-2 at Thr-555 (Fig. 6A). The phosphorylation increased up to about sixfold more than the basal level during the first 3 min (Fig. 6A and B). To examine whether ephrin-A5-induced phosphorylation of CRMP-2 at Thr-555 was mediated by Rho kinase, DRG neurons were stimulated by ephrin-A5 in the presence of Rho kinase inhibitor (Y-27632 or HA1077) for 1 h (69). Y-27632 and HA1077 inhibited the ephrin-A5-induced phosphorylation of CRMP-2 (Fig. 6A and B). These results indicate that CRMP-2 is phosphorylated at Thr-555 by Rho kinase during ephrin-A5-induced growth cone collapse of DRG neurons, as well during as during that induced by LPA, as reported previously (5). We then examined the localization of phosphorylated CRMP-2 after the stimulation with ephrin-

FIG. 4. Electron microscopic immunocytochemical localization of CRMP-2 in chick DRG growth cones. (A to C) Horizontal section of central area of growth cones. Enlarged images from insets a to c in panels A to C are shown in panels a to c. In panels a and b, red arrows indicate the immunolabeling of CRMP-2. Thin lines are microtubule filaments. (B) Grazing section of growth cones. Red arrows indicate the immunolabeling of CRMP-2 close to the plasma membrane. (C) Immunolabeling with anti-phospho-CRMP-2 was not observed. Bars (panels a to c), 500 nm. (D to H) High-power view of the sample prepared by freeze-etching immunoreplica methods (negative images are shown for clarity). Immunocolloidal gold is shown as white dots. Red arrows indicate the immunolabeling of CRMP-2 on clathrin-coated pits (D and E) and on actin filaments (G) or of phosphorylated CRMP-2 on actin filaments (H). Immunolabeling with anti-phospho-CRMP-2 antibody was not observed on clathrin-coated pits (F). Bar (D to H), 50 nm.

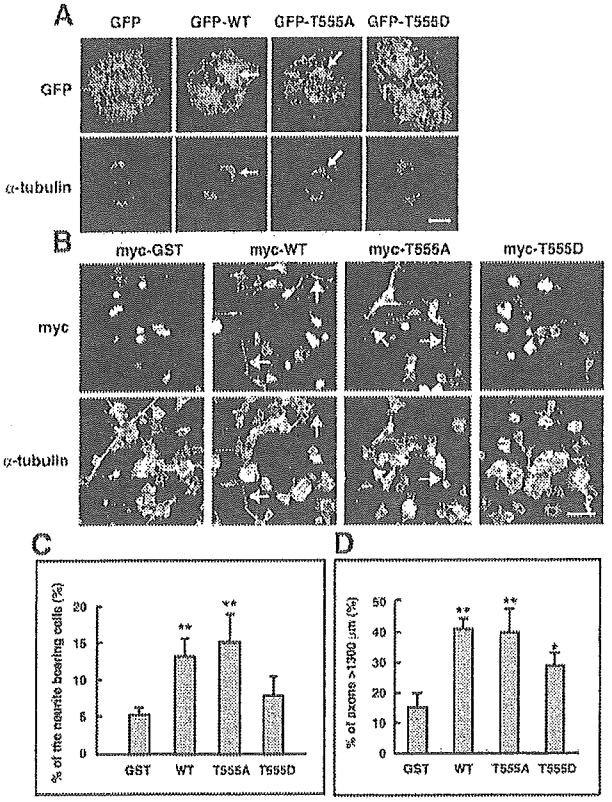

FIG. 5. Effects of CRMP-2 mutants on neurite formation in N1E-115 cells and DRG neurons. (A) Localization of GFP-tagged CRMP-2 and CRMP-2 mutants T555A and T555D. Vero cells were transfected with pEGFP-CRMP-2 WT, T555A, or T555D and cultured for 36 h. Transfected cells were fixed and stained with anti-α-tubulin antibody. Arrows indicate the colocalization of GFP-fused protein with microtubules. Bar, 10 μm. (B) The effect of overexpression of CRMP-2 WT, T555A, and T555D on process formation in N1E-115 cells. N1E-115 cells were transfected with myc-GST (as a negative control), CRMP-2 WT, T555A, or T555D. Twenty-four hours after transfection, the cells were cultured in serum-containing medium for 24 h. Transfected cells were fixed and doubly stained by anti-myc antibody (top panels) and anti-α-tubulin antibody (bottom panels). Arrows indicate the processes induced by CRMP-2 constructs. Bar, 40 μm. (C) The percentage of cells bearing neurites (length > 20 μm) in transfected cells. Fifty randomly selected transfected neurons were quantified for each construct. The values shown are means ± standard errors of triplicate experiments. **, significantly different from the cells expressing GST as analyzed by Student's *t* test ($P < 0.01$). (D) The percentage of cells bearing axons (length > 1,300 μm) in DRG neuron-transfected cells. DRG neurons were transfected with the plasmids indicated in panel B. After transfection, the neurons were cultured in the NGF-deprived medium for 3 days. Transfected neurons were fixed and doubly stained by anti-myc antibody and anti-neurofilament antibody. The percentage of neurons bearing axons with length > 1,300 μm versus the total number of neurons bearing axons was analyzed. Fifty randomly selected transfected neurons were quantified for each construct. The values shown are means ± standard errors of triplicate experiments. **, significantly different from the cells expressing GST as analyzed by Student's *t* test ($P < 0.01$); *, $P < 0.05$.

A5. Because ephrin-A5 treatment makes the growth cone collapse, the relative amount of increased phosphorylation of CRMP-2 could not be measured in spreading growth cones (data not shown). However, higher immunolabeling of phosphorylated CRMP-2 was observed in collapsed growth cones (Fig. 6C and D). Y-27632 prevented the growth cone collapse, as reported previously (71), and inhibited an increase of phosphorylated CRMP-2 levels at the tips of axons (data not shown). Staining by the phospho-CRMP-2 antibody was visible as dot-like structures in both the growth cone and axon shaft compared to the results seen with CRMP-2 antibody. The nature of this dot-like structure has not been elucidated.

To examine the role of CRMP-2 phosphorylation in growth cone morphology, we expressed the CRMP-2 mutants T555A and T555D in DRG neurons. The expression of CRMP-2 WT had no effect on ephrin-A5-induced growth cone collapse compared to the control results, whereas the expression of the mutant CRMP-2 T555A partially inhibited ephrin-A5-induced growth cone collapse ($P < 0.05$; Fig. 6C, bottom panel). These results suggest that phosphorylation of CRMP-2 at Thr-555 is partially involved in ephrin-A5-induced growth cone collapse. Of note, the effect of the T555A mutant is not complete, because the endogenous CRMP-2 expression level is relatively high in DRG neurons (39), and the nonphosphorylated form of CRMP-2 may not completely replace endogenous CRMP-2. In addition, a lot of substrates of Rho kinase have been reported and are expected to participate partially in growth cone collapse, as previously reported (71). Finally, it should be noted that the expression of CRMP-2 T555D increased the number of collapsed growth cones and slightly inhibited ephrin-A5-induced growth cone collapse. Although the exact mode of action of CRMP-2 T555D is not known, this mutant may mimic phosphorylated CRMP-2 and induce growth cone collapse while partially inhibiting Rho kinase activity in a manner competitive with endogenous CRMP-2.

DISCUSSION

CRMP-2 was first reported as a mediator of Sema3A-induced growth cone collapse (31). However, the molecular mechanisms involving CRMP-2 in growth cone collapse have not been elucidated. We previously reported that Rho kinase phosphorylates CRMP-2 at Thr-555 during LPA-induced, but not Sema3A-induced, growth cone collapse in DRG neurons (5) and that overexpression of CRMP-2 in hippocampal neurons enhances axon formation by its association with tubulin heterodimer and Numb (28, 34, 39, 56). CRMP-2 functions as a carrier of tubulin heterodimers, which delivers tubulin dimers to the assembly plus ends of nucleating sites or growing microtubules (28). CRMP-2 associates with Numb and regulates L1 endocytosis at axonal growth cones in hippocampal neurons (56). Although these reports revealed that CRMP-2 functions in axon elongation, the molecular mechanisms involving CRMP-2 and its interacting molecules in growth cone collapse remain unresolved. And we also reported the involvement of phosphorylation at Thr-514 by GSK-3β in neuronal polarity and that Thr-522 was phosphorylated by Cdk5 downstream of Sema3A (68, 73) but have not investigated the meaning of these phosphorylation events with respect to the growth cone collapse. In the present study, we found that phosphorylation by Rho kinase inhibits the ability of CRMP-2 to bind tubulin and Numb. These interactions are necessary for growth cone advance and axon growth. Therefore, we suggest that ephrin-A5 stimulation dissociates CRMP-2 from interacting

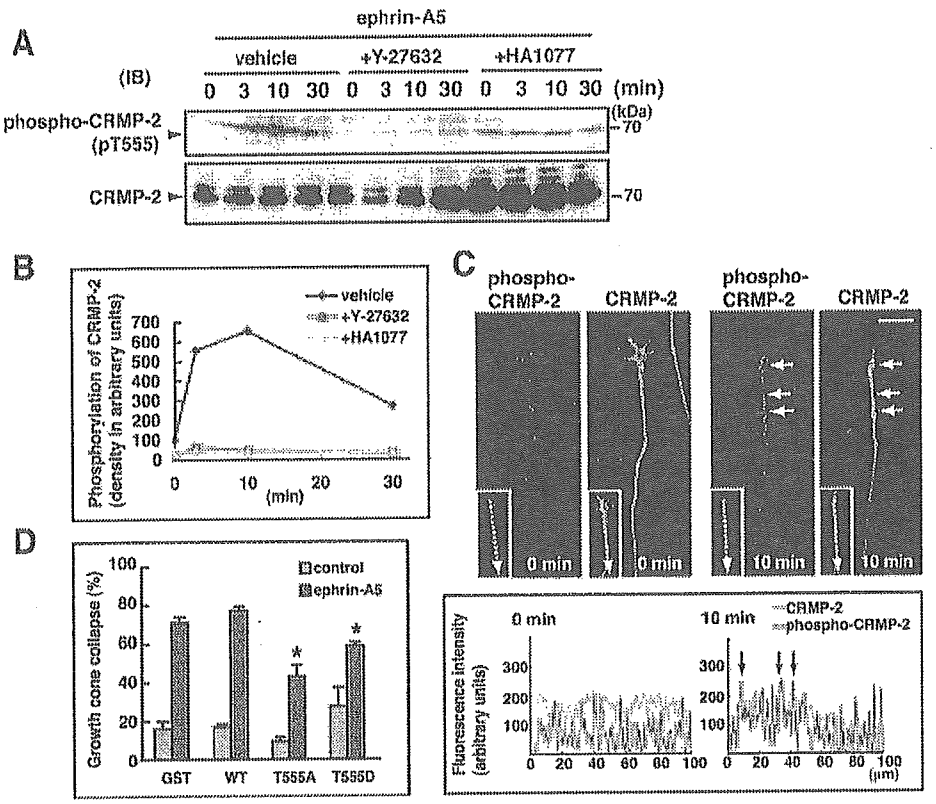

FIG. 6. Ephrin-A5-induced CRMP-2 phosphorylation. (A) DRG neurons were serum starved for 4 h and stimulated by 1 μg/ml ephrin-A5 with or without pretreatment with 10 μM Rho kinase inhibitor (Y-27632 or HA1077) for 0, 3, 10, and 30 min. The cell lysate was resolved by SDS-PAGE and immunoblotted (IB) with the indicated antibodies. The multiple bands of CRMP-2 represent differentially phosphorylated forms (33). Arrowheads indicate the intact protein of CRMP-2. The band corresponding to the phosphorylated form by Rho kinase was detected at the same position as the main band detected by anti-CRMP-2 antibody. The results are representative of three independent experiments. (B) The relative levels resulting from CRMP-2 phosphorylation were calculated, with the level obtained with untreated control cells defined as 100 units. (C) The localization of phosphorylated CRMP-2 before and after stimulation with ephrin-A5 in DRG neurons. DRG neurons were serum starved for 4 h and stimulated by 1 μg/ml ephrin-A5. Before stimulation and 10 min after stimulation with ephrin-A5, cells were fixed and immunostained with anti-phospho-CRMP-2 antibody (red) and anti-CRMP-2 antibody (green). Arrows indicate the collapsed growth cone and axonal shaft, which was intensely stained by anti-phospho-CRMP-2 antibody. Bar, 20 μm. The fluorescence intensities of CRMP-2 (green) and phospho-CRMP-2 (red) in the dotted lines are shown in the graphs (bottom panel). Arrows indicate the same positions as the areas indicated by arrows in the images (upper panels). (D) Effects of CRMP-2 mutants T555A and T555D on ephrin-A5-induced growth cone collapse. DRG neurons transfected with myc-GST, CRMP-2 WT, T555A, or T555D were stimulated with ephrin-A5 for 30 min. Then the population of collapsed growth cones expressing introduced constructs was calculated. Thirty randomly selected transfected neurons were quantified for each construct. The values shown are means ± standard errors of triplicate experiments. *, significantly different from the growth cones expressing GST as analyzed by Student's t test ($P < 0.05$).

molecules by phosphorylation and enhances growth cone collapse.

In previous reports, we showed that CRMP-2 enhances microtubule assembly and, thereby, axon formation (28). And here we report that the phosphorylation by Rho kinase prevents the association with tubulin dimer-microtubules. This regulation of CRMP-2 activity seems to cause the reduction of microtubule assembly. The plus ends of microtubules in growth cones exhibit a property termed dynamic instability, wherein they cycle through periods of growth and shrinkage (6, 27, 53, 65). The increase of microtubule assembly is required for the growth cone advance (27, 28). In fact, some groups showed that the polymerization and capturing of microtubules in one direction and the shrinkage of microtubules in the other direction are early steps in guidance of axonal growth cones, suggesting that the regulation of microtubule dynamic instability is closely related to the morphological changes of growth cones (11, 60, 66, 76). Therefore, the enhancement of microtubule assembly by CRMP-2 is critical for the growth cone dynamics. The canceling of the interaction of CRMP-2 and tubulin dimer and/or microtubules by phosphorylation is thought to prevent the proper microtubule formation. Taken together, these data indicate that the negative regulation of CRMP-2 activity appears to disrupt the normal microtubule dynamics, followed by the collapse of growth cone morphology.

Knockdown of CRMP-2 in hippocampal neurons inhibits Numb-mediated L1 endocytosis and axon growth (56). Here we report that phosphorylated CRMP-2 could not associate with Numb. Thus, it is possible that CRMP-2 phosphorylation also inhibits Numb-mediated L1 endocytosis. However, two groups have reported that growth cone collapse triggered by Sema3A or ephrins was accompanied by enhanced endocytosis (26, 41); they observed the fluorescence-labeled dextran uptake or reorganization of signaling molecules neuropilin 1

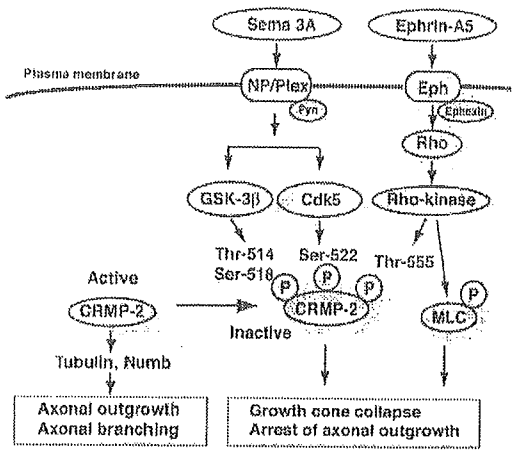

FIG. 7. Model schema for the phosphorylation of CRMP-2 by Rho kinase, Cdk5, and GSK-3β. Sema3A is thought to activate Cdk5 and GSK-3β. These activations cause phosphorylation at Ser-522, Ser-518, and Thr-514. Ephrin-A5 stimulation activates the Rho/Rho kinase signaling pathway and subsequently induces the phosphorylation of CRMP-2 at Thr-555 by Rho kinase. The binding activity of CRMP-2 to tubulin is decreased by the phosphorylation by Cdk5, GSK-3β, and Rho kinase. Nonphosphorylated CRMP-2 binds to tubulin heterodimers to promote microtubule assembly or Numb-mediated endocytosis, thereby enhancing axon elongation and branching. In contrast, the phosphorylated form cannot associate with interacting molecules and loses the positive effect on axon elongation, thereby causing arrest of axon growth and growth cone collapse.

(NP1), plexin, and Rac in response to guidance cues. In a reconstituted Sema3A signaling system in COS-7 cells expressing the receptor components NP1 and plexin A1, CRMP and plexin A1 form a physical complex and CRMP accelerates Sema3A-induced cell contraction (17). In contrast, NGF signaling increases clathrin-coated membrane formation and clathrin-mediated membrane trafficking, as revealed by the increased endocytosis of transferrin (7). Judging from these reports, endocytosis appears to be selectively regulated for axon outgrowth and growth cone collapse. L1 and L1 recycling are crucial for axon elongation and growth cone motility (43). Inactivation of CRMP-2 may be required for the selective inhibition of cell adhesion molecules to prevent the growth cone dynamics. Although the exact mechanisms causing growth cone collapse need additional study, our results imply that ephrin-A5-induced growth cone collapse is enhanced by the CRMP-2 phosphorylation through the inhibition of Numb-mediated endocytosis.

CRMP-2 is implicated in Sema3A-induced growth cone collapse (31). The phosphorylation of CRMP-2 at Thr-555 by Rho kinase was observed during LPA-induced growth cone collapse but not during Sema3A-induced collapse (5). In retinal ganglion cells, ephrin-A5-induced growth cone collapse is mediated by Rho kinase (13, 71). In the present study, we found that Rho kinase phosphorylates CRMP-2 at Thr-555 in response to ephrin-A5. It has been reported that activation of Fyn, Cdk5, and GSK-3β is involved in Sema3A signaling (22, 62) (Fig. 7). Activated Cdk5 phosphorylates Tau and causes microtubule reorganization induced by Sema3A (62). Recently, our group and several other groups have reported that CRMP-2 is phosphorylated by Cdk5, dual tyrosine-regulated kinase (DYRK), and GSK-3β (10, 14, 73). Cdk5 and DYRK phosphorylate CRMP-2 at Ser-522, and this phosphorylation site acts as a priming site for subsequent GSK-3β phosphorylation at Ser-518 and Thr-514. Here, we found that the phosphorylation of CRMP-2 by Cdk5 and GSK-3β cancels the binding activity to tubulin and Numb. Thus, both signaling pathways downstream of Sema3A and ephrin-A5 as well as LPA seem to terminate in the same molecule, CRMP-2, through activation by different kinases, followed by microtubule reorganization (Fig. 7). On the other hand, we reported that neurotropic factors BDNF and NT-3, but not NGF, inhibit the phosphorylation of CRMP-2 via PI 3-kinase and Akt in hippocampal neurons (73). These growth factors are known to prevent growth cone collapse in response to the repulsive guidance cues (20, 67). Thus, it appears that attractive and repulsive extracellular cues regulate the balance of phosphorylation and dephosphorylation in CRMP-2, thereby managing microtubule formation and endocytosis. The function of CRMP-2 would be dramatically regulated by several kinds of kinases in response to extracellular stimulation.

Rho kinase has multiple substrates regulating the dynamics of the actin filament (35, 42). Rho kinase regulates the phosphorylation of MLC, resulting in actomyosin contractility, which is observed during ephrin-A5-induced growth cone collapse (71). We recently found that Rho kinase phosphorylates the microtubule-associated proteins (MAPs) Tau and MAP-2 (3, 4). This phosphorylation dissociates MAPs from microtubule filaments in neurons. In fact, in this study the mutant that mimicked CRMP-2 phosphorylated by Rho kinase could not inhibit the ephrin-A5-induced growth cone collapse completely, suggesting that Rho kinase is likely to phosphorylate multiple substrates, including MLC and MAPs, to achieve growth cone collapse. Because nonphosphorylated CRMP-2 can enhance the assembly of microtubules, we speculate that phosphorylated CRMP-2 may lose the ability to drive the microtubule formation, thus causing the destabilization of microtubule formation, in association with phosphorylated MAPs.

We found actin to be a CRMP-2-interacting protein. Both phosphorylated and nonphosphorylated forms of CRMP-2 bound to actin in vitro, and CRMP-2 was detected on actin filaments in DRG neuron growth cones. We examined whether CRMP-2 associates with actin monomer in vitro by use of purified actin monomers and recombinant CRMP-2 proteins, but a direct association was not observed. In another study, we have recently found that CRMP-2 interacts with Specifically Rac1-Associated protein (Sra-1/CYFIP1) (43a), which directly interacts with actin filaments (45). Thus, CRMP-2 may associate with actin filaments through Sra-1 in growth cones. In this study, Rho kinase-induced phosphorylation of CRMP-2 had no effect on the actin binding ability of CRMP-2. CRMP-2 is a highly conserved phosphoprotein, and its phosphorylation states alter upon NGF-induced neuronal differentiation or in the formation of degenerating neurites in the brains of patients with Alzheimer's disease (12, 33). These findings raise the possibility that other kinases up- or down-regulate CRMP-2 activity and mediate actin reorganization in the Rho family GTPase-mediated signal cascade. Further studies characterizing the protein kinases may shed some light on other functions of CRMP-2.

ACKNOWLEDGMENTS

We thank Y. Gu, Y. Ihara, E. Mekada, T. Kato, and H. Tanaka for their kind gifts of materials. We also thank T. Nishimura and N. Mishima Yoshimura (Nagoya University) for helpful discussion and preparing some materials and T. Ishii for secretarial and technical assistance.

This work was supported by Grants-in-Aid for scientific research from the Ministry of Education, Culture, Sports, Science and Technology of Japan, a Grant-in-Aid for Creative Scientific Research from the Ministry of Education, Culture, Sports, Science and Technology of Japan (MEXT), Special Coordination Funds for Promoting Science and Technology (SCFPST), National Institute of Biomedical Innovation, Research Fellowships of the Japan Society for the Promotion of Science for Young Scientists (JSPS), the 21st Century Centre of Excellence (COE) Program from MEXT, and a Research Grant (15A-2) for Nervous and Mental Disorders from the Ministry of Health, Labor and Welfare.

REFERENCES

1. **Amano, M., K. Chihara, N. Nakamura, Y. Fukata, T. Yano, M. Shibata, M. Ikebe, and K. Kaibuchi.** 1998. Myosin II activation promotes neurite retraction during the action of Rho and Rho-kinase. Genes Cells **3**:177–188.
2. **Amano, M., M. Ito, K. Kimura, Y. Fukata, K. Chihara, T. Nakano, Y. Matsuura, and K. Kaibuchi.** 1996. Phosphorylation and activation of myosin by Rho-associated kinase (Rho-kinase). J. Biol. Chem. **271**:20246–20249.
3. **Amano, M., T. Kaneko, A. Maeda, M. Nakayama, M. Ito, T. Yamauchi, H. Goto, Y. Fukata, N. Oshiro, A. Shinohara, A. Iwamatsu, and K. Kaibuchi.** 2003. Identification of Tau and MAP2 as novel substrates of Rho-kinase and myosin phosphatase. J. Neurochem. **87**:780–790.
4. **Amano, M., Y. Fukata, and K. Kaibuchi.** 2000. Regulation and functions of Rho-associated kinase. Exp. Cell Res. **261**:44–51.
5. **Arimura, N., N. Inagaki, K. Chihara, C. Menager, N. Nakamura, M. Amano, A. Iwamatsu, Y. Goshima, and K. Kaibuchi.** 2000. Phosphorylation of collapsin response mediator protein-2 by Rho-kinase. Evidence for two separate signaling pathways for growth cone collapse. J. Biol. Chem. **275**:23973–23980.
6. **Baas, P. W., M. M. Black, and G. A. Banker.** 1989. Changes in microtubule polarity orientation during the development of hippocampal neurons in culture. J. Cell Biol. **109**:3085–3094.
7. **Beattie, E. C., C. L. Howe, A. Wilde, F. M. Brodsky, and W. C. Mobley.** 2000. NGF signals through TrkA to increase clathrin at the plasma membrane and enhance clathrin-mediated membrane trafficking. J. Neurosci. **20**:7325–7333.
8. **Berninger, B., D. E. Garcia, N. Inagaki, C. Hahnel, and D. Lindholm.** 1993. BDNF and NT-3 induce intracellular $Ca2^+$ elevation in hippocampal neurones. Neuroreport **4**:1303–1306.
9. **Bito, H., T. Furuyashiki, H. Ishihara, Y. Shibasaki, K. Ohashi, K. Mizuno, M. Maekawa, T. Ishizaki, and S. Narumiya.** 2000. A critical role for a Rho-associated kinase, p160ROCK, in determining axon outgrowth in mammalian CNS neurons. Neuron **26**:431–441.
10. **Brown, M., T. Jacobs, B. Eickholt, G. Ferrari, M. Teo, C. Monfries, R. Z. Qi, T. Leung, L. Lim, and C. Hall.** 2004. Alpha2-chimaerin, cyclin-dependent kinase 5/p35, and its target collapsin response mediator protein-2 are essential components in semaphorin 3A-induced growth-cone collapse. J. Neurosci. **24**:8994–9004.
11. **Buck, K. B., and J. Q. Zheng.** 2002. Growth cone turning induced by direct local modification of microtubule dynamics. J. Neurosci. **22**:9358–9367.
12. **Byk, T., S. Ozon, and A. Sobel.** 1998. The Ulip family phosphoproteins—common and specific properties. Eur. J. Biochem. **254**:14–24.
13. **Cheng, Q., Y. Sasaki, M. Shoji, Y. Sugiyama, H. Tanaka, T. Nakayama, N. Mizuki, F. Nakamura, K. Takei, and Y. Goshima.** 2003. Cdk5/p35 and Rho-kinase mediate ephrin-A5-induced signaling in retinal ganglion cells. Mol. Cell. Neurosci. **24**:632–645.
14. **Cole, A. R., A. Knebel, N. A. Morrice, L. S. Robertson, A. J. Irving, C. N. Connolly, and C. Sutherland.** 2004. GSK-3 phosphorylation of the Alzheimer epitope within collapsin response mediator proteins regulates axon elongation in primary neurons. J. Biol. Chem. **279**:50176–50180.
15. **Dean, A. M., and D. E. Koshland, Jr.** 1990. Electrostatic and steric contributions to regulation at the active site of isocitrate dehydrogenase. Science **249**:1044–1046.
16. **Dent, E. W., and F. B. Gertler.** 2003. Cytoskeletal dynamics and transport in growth cone motility and axon guidance. Neuron **40**:209–227.
17. **Deo, R. C., E. F. Schmidt, A. Elhabazi, H. Togashi, S. K. Burley, and S. M. Strittmatter.** 2004. Structural bases for CRMP function in plexin-dependent semaphorin3A signaling. EMBO J. **23**:9–22.
18. **Diefenbach, T. J., P. B. Guthrie, H. Stier, B. Billups, and S. B. Kater.** 1999. Membrane recycling in the neuronal growth cone revealed by FM1-43 labeling. J. Neurosci. **19**:9436–9444.
19. **Donoghue, M. J., R. M. Lewis, J. P. Merlie, and J. R. Sanes.** 1996. The Eph kinase ligand AL-1 is expressed by rostral muscles and inhibits outgrowth from caudal neurons. Mol. Cell. Neurosci. **8**:185–198.
20. **Dontchev, V. D., and P. C. Letourneau.** 2002. Nerve growth factor and semaphorin 3A signaling pathways interact in regulating sensory neuronal growth cone motility. J. Neurosci. **22**:6659–6669.
21. **Drescher, U., F. Bonhoeffer, and B. K. Muller.** 1997. The Eph family in retinal axon guidance. Curr. Opin. Neurobiol. **7**:75–80.
22. **Eickholt, B. J., F. S. Walsh, and P. Doherty.** 2002. An inactive pool of GSK-3 at the leading edge of growth cones is implicated in semaphorin 3A signaling. J. Cell Biol. **157**:211–217.
23. **Fan, J., and J. A. Raper.** 1995. Localized collapsing cues can steer growth cones without inducing their full collapse. Neuron **14**:263–274.
24. **Flanagan, J. G., and P. Vanderhaeghen.** 1998. The ephrins and Eph receptors in neural development. Annu. Rev. Neurosci. **21**:309–345.
25. **Fong, Y. L., W. L. Taylor, A. R. Means, and T. R. Soderling.** 1989. Studies of the regulatory mechanism of $Ca2^+$/calmodulin-dependent protein kinase II. Mutation of threonine 286 to alanine and aspartate. J. Biol. Chem. **264**: 16759–16763.
26. **Fournier, A. E., F. Nakamura, S. Kawamoto, Y. Goshima, R. G. Kalb, and S. M. Strittmatter.** 2000. Semaphorin3A enhances endocytosis at sites of receptor-F-actin colocalization during growth cone collapse. J. Cell Biol. **149**:411–422.
27. **Fukata, M., M. Nakagawa, and K. Kaibuchi.** 2003. Roles of Rho-family GTPases in cell polarisation and directional migration. Curr. Opin. Cell Biol. **15**:590–597.
28. **Fukata, Y., T. J. Itoh, T. Kimura, C. Menager, T. Nishimura, T. Shiromizu, H. Watanabe, N. Inagaki, A. Iwamatsu, H. Hotani, and K. Kaibuchi.** 2002. CRMP-2 binds to tubulin heterodimers to promote microtubule assembly. Nat. Cell Biol. **4**:583–591.
29. **Ganju, P., K. Shigemoto, J. Brennan, A. Entwistle, and A. D. Reith.** 1994. The Eck receptor tyrosine kinase is implicated in pattern formation during gastrulation, hindbrain segmentation and limb development. Oncogene **9**:1613–1624.
30. **Goshima, Y., T. Kawakami, H. Hori, Y. Sugiyama, S. Takasawa, Y. Hashimoto, M. Kagoshima-Maezono, T. Takenaka, Y. Misu, and S. M. Strittmatter.** 1997. A novel action of collapsin: collapsin-1 increases antero- and retrograde axoplasmic transport independently of growth cone collapse. J. Neurobiol. **33**:316–328.
31. **Goshima, Y., F. Nakamura, P. Strittmatter, and S. M. Strittmatter.** 1995. Collapsin-induced growth cone collapse mediated by an intracellular protein related to UNC-33. Nature **376**:509–514.
32. **Grunwald, I. C., and R. Klein.** 2002. Axon guidance: receptor complexes and signaling mechanisms. Curr. Opin. Neurobiol. **12**:250–259.
33. **Gu, Y., N. Hamajima, and Y. Ihara.** 2000. Neurofibrillary tangle-associated collapsin response mediator protein-2 (CRMP-2) is highly phosphorylated on Thr-509, Ser-518, and Ser-522. Biochemistry **39**:4267–4275.
34. **Gu, Y., and Y. Ihara.** 2000. Evidence that collapsin response mediator protein-2 is involved in the dynamics of microtubules. J. Biol. Chem. **275**:17917–17920.
35. **Hall, A.** 1998. Rho GTPases and the actin cytoskeleton. Science **279**:509–514.
36. **Hall, A., and C. D. Nobes.** 2000. Rho GTPases: molecular switches that control the organization and dynamics of the actin cytoskeleton. Philos. Trans. R. Soc. Lond. B Biol. Sci. **355**:965–970.
37. **Hedgecock, E. M., J. G. Culotti, J. N. Thomson, and L. A. Perkins.** 1985. Axonal guidance mutants of *Caenorhabditis elegans* identified by filling sensory neurons with fluorescein dyes. Dev. Biol. **111**:158–170.
38. **Hirose, M., T. Ishizaki, N. Watanabe, M. Uehata, O. Kranenburg, W. H. Moolenaar, F. Matsumura, M. Maekawa, H. Bito, and S. Narumiya.** 1998. Molecular dissection of the Rho-associated protein kinase (p160ROCK)-regulated neurite remodeling in neuroblastoma N1E-115 cells. J. Cell Biol. **141**:1625–1636.
39. **Inagaki, N., K. Chihara, N. Arimura, C. Menager, Y. Kawano, N. Matsuo, T. Nishimura, M. Amano, and K. Kaibuchi.** 2001. CRMP-2 induces axons in cultured hippocampal neurons. Nat. Neurosci. **4**:781–782.
40. **Ishizaki, T., M. Maekawa, K. Fujisawa, K. Okawa, A. Iwamatsu, A. Fujita, N. Watanabe, Y. Saito, A. Kakizuka, N. Morii, and S. Narumiya.** 1996. The small GTP-binding protein Rho binds to and activates a 160 kDa Ser/Thr protein kinase homologous to myotonic dystrophy kinase. EMBO J. **15**: 1885–1893.
41. **Jurney, W. M., G. Gallo, P. C. Letourneau, and S. C. McLoon.** 2002. Rac1-mediated endocytosis during ephrin-A2- and semaphorin 3A-induced growth cone collapse. J. Neurosci. **22**:6019–6028.
42. **Kaibuchi, K., S. Kuroda, and M. Amano.** 1999. Regulation of the cytoskeleton and cell adhesion by the Rho family GTPases in mammalian cells. Annu. Rev. Biochem. **68**:459–486.
43. **Kamiguchi, H., and V. Lemmon.** 2000. Recycling of the cell adhesion molecule L1 in axonal growth cones. J. Neurosci. **20**:3676–3686.

43a. **Kawano, Y., T. Yoshimura, D. Tsuboi, S. Kawabata, T. Kaneko-Kawano, H. Shirataki, T. Takenawa, and K. Kaibuchi.** 2005. CRMP-2 is involved in kinesin-1-dependent transport of the Sra-1/WAVE1 complex and axon formation. Mol. Cell. Biol. **25**:9920–9935.

44. **Knoll, B., and U. Drescher.** 2004. Src family kinases are involved in EphA receptor-mediated retinal axon guidance. J. Neurosci. 24:6248–6257.
45. **Kobayashi, K., S. Kuroda, M. Fukata, T. Nakamura, T. Nagase, N. Nomura, Y. Matsuura, N. Yoshida-Kubomura, A. Iwamatsu, and K. Kaibuchi.** 1998. p140Sra-1 (specifically Rac1-associated protein) is a novel specific target for Rac1 small GTPase. J. Biol. Chem. 273:291–295.
46. **Kullander, K., and R. Klein.** 2002. Mechanisms and functions of Eph and ephrin signalling. Nat. Rev. Mol. Cell Biol. 3:475–486.
47. **Kurland, I. J., M. R. el-Maghrabi, J. J. Correia, and S. J. Pilkis.** 1992. Rat liver 6-phosphofructo-2-kinase/fructose-2,6-bisphosphatase. Properties of phospho- and dephospho- forms and of two mutants in which Ser32 has been changed by site-directed mutagenesis. J. Biol. Chem. 267:4416–4423.
48. **Lai, K. O., F. C. Ip, and N. Y. Ip.** 1999. Identification and characterization of splice variants of ephrin-A3 and ephrin-A5. FEBS Lett. 458:265–269.
49. **Li, W., R. K. Herman, and J. E. Shaw.** 1992. Analysis of the *Caenorhabditis elegans* axonal guidance and outgrowth gene unc-33. Genetics 132:675–689.
50. **Liu, X., K. Seno, Y. Nishizawa, F. Hayashi, A. Yamazaki, H. Matsumoto, T. Wakabayashi, and J. Usukura.** 1994. Ultrastructural localization of retinal guanylate cyclase in human and monkey retinas. Exp. Eye Res. 59:761–768.
51. **Mack, T. G., M. P. Koester, and G. E. Pollerberg.** 2000. The microtubule-associated protein MAP1B is involved in local stabilization of turning growth cones. Mol. Cell. Neurosci. 15:51–65.
52. **Matsuura, Y., R. D. Possee, H. A. Overton, and D. H. Bishop.** 1987. Baculovirus expression vectors: the requirements for high level expression of proteins, including glycoproteins. J. Gen. Virol. 68(Pt. 5):1233–1250.
53. **Mitchison, T., and M. Kirschner.** 1984. Dynamic instability of microtubule growth. Nature 312:237–242.
54. **Mitsui, N., R. Inatome, S. Takahashi, Y. Goshima, H. Yamamura, and S. Yanagi.** 2002. Involvement of Fes/Fps tyrosine kinase in semaphorin3A signaling. EMBO J. 21:3274–3285.
55. **Mueller, B. K.** 1999. Growth cone guidance: first steps towards a deeper understanding. Annu. Rev. Neurosci. 22:351–388.
56. **Nishimura, T., Y. Fukata, K. Kato, T. Yamaguchi, Y. Matsuura, H. Kamiguchi, and K. Kaibuchi.** 2003. CRMP-2 regulates polarized Numb-mediated endocytosis for axon growth. Nat. Cell Biol. 5:819–826.
57. **Ohta, K., H. Iwamasa, U. Drescher, H. Terasaki, and H. Tanaka.** 1997. The inhibitory effect on neurite outgrowth of motoneurons exerted by the ligands ELF-1 and RAGS. Mech. Dev. 64:127–135.
58. **Quinn, C. C., E. Chen, T. G. Kinjo, G. Kelly, A. W. Bell, R. C. Elliott, P. S. McPherson, and S. Hockfield.** 2003. TUC-4b, a novel TUC family variant, regulates neurite outgrowth and associates with vesicles in the growth cone. J. Neurosci. 23:2815–2823.
59. **Raper, J. A., and J. P. Kapfhammer.** 1990. The enrichment of a neuronal growth cone collapsing activity from embryonic chick brain. Neuron 4:21–29.
60. **Sabry, J. H., T. P. O'Connor, L. Evans, A. Toroian-Raymond, M. Kirschner, and D. Bentley.** 1991. Microtubule behavior during guidance of pioneer neuron growth cones in situ. J. Cell Biol. 115:381–395.
61. **Sahin, M., P. L. Greer, M. Z. Lin, H. Poucher, J. Eberhart, S. Schmidt, T. M. Wright, S. M. Shamah, S. O'Connell, C. W. Cowan, L. Hu, J. L. Goldberg, A. Debant, G. Corfas, C. E. Krull, and M. E. Greenberg.** 2005. Eph-dependent tyrosine phosphorylation of ephexin1 modulates growth cone collapse. Neuron 46:191–204.
62. **Sasaki, Y., C. Cheng, Y. Uchida, O. Nakajima, T. Ohshima, T. Yagi, M. Taniguchi, T. Nakayama, R. Kishida, Y. Kudo, S. Ohno, F. Nakamura, and Y. Goshima.** 2002. Fyn and Cdk5 mediate semaphorin-3A signaling, which is involved in regulation of dendrite orientation in cerebral cortex. Neuron 35:907–920.
63. **Shamah, S. M., M. Z. Lin, J. L. Goldberg, S. Estrach, M. Sahin, L. Hu, M. Bazalakova, R. L. Neve, G. Corfas, A. Debant, and M. E. Greenberg.** 2001. EphA receptors regulate growth cone dynamics through the novel guanine nucleotide exchange factor ephexin. Cell 105:233–244.
64. **Song, H. J., and M. M. Poo.** 1999. Signal transduction underlying growth cone guidance by diffusible factors. Curr. Opin. Neurobiol. 9:355–363.
65. **Tanaka, E., T. Ho, and M. W. Kirschner.** 1995. The role of microtubule dynamics in growth cone motility and axonal growth. J. Cell Biol. 128:139–155.
66. **Tanaka, E., and M. W. Kirschner.** 1995. The role of microtubules in growth cone turning at substrate boundaries. J. Cell Biol. 128:127–137.
67. **Tuttle, R., and D. D. O'Leary.** 1998. Neurotrophins rapidly modulate growth cone response to the axon guidance molecule, collapsin-1. Mol. Cell. Neurosci. 11:1–8.
68. **Uchida, Y., T. Ohshima, Y. Sasaki, H. Suzuki, S. Yanai, N. Yamashita, F. Nakamura, K. Takei, Y. Ihara, K. Mikoshiba, P. Kolattukudy, J. Honnorat, and Y. Goshima.** 2005. Semaphorin3A signalling is mediated via sequential Cdk5 and GSK3beta phosphorylation of CRMP2: implication of common phosphorylating mechanism underlying axon guidance and Alzheimer's disease. Genes Cells 10:165–179.
69. **Uehata, M., T. Ishizaki, H. Satoh, T. Ono, T. Kawahara, T. Morishita, H. Tamakawa, K. Yamagami, J. Inui, M. Maekawa, and S. Narumiya.** 1997. Calcium sensitization of smooth muscle mediated by a Rho-associated protein kinase in hypertension. Nature 389:990–994.
70. **Usukura, J., and D. Bok.** 1987. Changes in the localization and content of opsin during retinal development in the rds mutant mouse: immunocytochemistry and immunoassay. Exp. Eye Res. 45:501–515.
71. **Wahl, S., H. Barth, T. Ciossek, K. Aktories, and B. K. Mueller.** 2000. Ephrin-A5 induces collapse of growth cones by activating Rho and Rho kinase. J. Cell Biol. 149:263–270.
72. **Wilkinson, D. G.** 2000. Eph receptors and ephrins: regulators of guidance and assembly. Int. Rev. Cytol. 196:177–244.
73. **Yoshimura, T., Y. Kawano, N. Arimura, S. Kawabata, A. Kikuchi, and K. Kaibuchi.** 2005. GSK-3beta regulates phosphorylation of CRMP-2 and neuronal polarity. Cell 120:137–149.
74. **Yuan, X. B., M. Jin, X. Xu, Y. Q. Song, C. P. Wu, M. M. Poo, and S. Duan.** 2003. Signalling and crosstalk of Rho GTPases in mediating axon guidance. Nat. Cell Biol. 5:38–45.
75. **Yuasa-Kawada, J., R. Suzuki, F. Kano, T. Ohkawara, M. Murata, and M. Noda.** 2003. Axonal morphogenesis controlled by antagonistic roles of two CRMP subtypes in microtubule organization. Eur. J. Neurosci. 17:2329–2343.
76. **Zheng, J. Q., J. J. Wan, and M. M. Poo.** 1996. Essential role of filopodia in chemotropic turning of nerve growth cone induced by a glutamate gradient. J. Neurosci. 16:1140–1149.

Adv Biochem Engin/Biotechnol (2005) 95: 1–15
DOI 10.1007/b102208
© Springer-Verlag Berlin Heidelberg 2005

Engineering Fluorescent Proteins

Atsushi Miyawaki (✉) · Takeharu Nagai · Hideaki Mizuno

Laboratory for Cell Function Dynamics, Advanced Technology Development Group, Brain Science Institute, RIKEN, 2-1 Hirosawa, Wako-city, Saitama, 351-0198 Japan
matsushi@brain.riken.jp

1 **Engineering for Brighter Fluorescence** 2
1.1 Fluorescence Development 2
1.2 Improvements in Maturation of YFP 5
1.3 Improvements in Maturation of DsRed 6

2 **Engineering for Photoactivation and Photoconversion** 7
2.1 Photoactivatable GFP 7
2.2 Kaede 8
2.3 Kindling Fluorescent Protein 9
2.4 Histidine for Photochemical Reactions 9

3 **Engineering for Disruption of Oligomerization** 9

4 **Engineering for Visualization of Cellular Functions** 11
4.1 Genetically-Encodable Probes 11
4.2 Voltage Sensors 11
4.3 Calcium Sensors 12

References 14

Abstract Green fluorescent protein from the jellyfish *Aequorea victora* (GFP) and GFP-like proteins from Anthozoa species encode light-absorbing chromophores intrinsically within their respective protein sequences. Recent studies have made progress in obtaining bright variants of these proteins which develop chromophores quickly and efficiently, as well as novel fluorescent proteins that photoactivate or photoconvert, i.e., become fluorescent or change colors upon illumination at specific wavelengths. Also, monomeric versions of these proteins have been engineered for fusion protein applications. Simple GFP variants and circularly permuted GFP variants have been used to develop fluorescent probes that sense physiological signals such as membrane potential and concentrations of free calcium. Further molecular characterization of the structure and maturation of these proteins is in progress, aimed at providing information for rational design of variants with desired fluorescence properties.

Keywords Green fluorescent protein · GFP-like proteins · Chromophore · Photoactivation · Photoconversion · Calcium imaging

List of Abbreviations

FP	Fluorescent protein
GFP	Green fluorescent protein
PA-GFP	Photoactivatable GFP
RFP	Red fluorescent protein
YFP	Yellow fluorescent protein

1 Engineering for Brighter Fluorescence

1.1 Fluorescence Development

Green fluorescent protein (GFP), originally isolated from the jellyfish *Aequorea victoria* (*Aequorea* GFP), has been the subject of continued interest since it was cloned in 1992 [1, 2]. Moreover, the discovery of novel GFP-like proteins from Anthozoans (coral animals) has significantly expanded the range of colors available for cell biological applications [3, 4]. Here, the term 'fluorescent protein' (FP) will be used to describe a protein that can become spontaneously fluorescent. Due to their autocatalytic chromophore generation, and the possibility of spectral manipulation of these proteins via mutagenesis, FPs of this sort make attractive tools for a myriad of biological applications. After protein synthesis, many FPs mature slowly through a multi-step process that consists of folding, chromophore formation, and chromophore modification. *Aequorea* GFP, for example, requires folding and chromophore formation processes, which for this protein may be interdependent [5]. Sometime during or after the protein adopts its native conformation, an internal tripeptide, Ser^{65}-Tyr^{66}-Gly^{67}, forms a chromophore, 4-(*p*-hydroxybenzylidene)-5-imidazolinone, by nucleophilic attack of Gly^{67}-Nα on the carbonyl group of Ser^{65}, followed by dehydration and oxidation of the α-β bond of Tyr^{66} (Fig. 1A). The wavelengths of light absorbed and emitted by the chromophore depend on the local chemistry, and as a result substitutions in or near the chromophore may produce large changes in fluorescence. Yellow fluorescent protein (YFP), a yellow variant of GFP, has a Tyr residue substituted at position Thr^{203} (T203Y). The π-π interaction between Tyr^{203} and the chromophore phenol ring most likely reduces the excited state energy, thereby increasing the excitation and emission wavelengths (Fig. 1B) [2]. In addition to folding and chromophore formation, some GFP-like proteins undergo a process of chromophore modification in order to reach a mature state with the desired fluorescence properties. This event takes place in the final folded molecule. For example, DsRed is a GFP-like protein that fluoresces first green and then red, implying that its chromophore structure is modified during maturation. Recent structural studies have shown that a tripeptide in DsRed (Gln^{66}-Tyr^{67}-Gly^{68}) analogous to the chromophore-forming sequence of *Aequorea* GFP forms a 4-(*p*-hydroxybenzylidene)-5-imidazolinone chro-

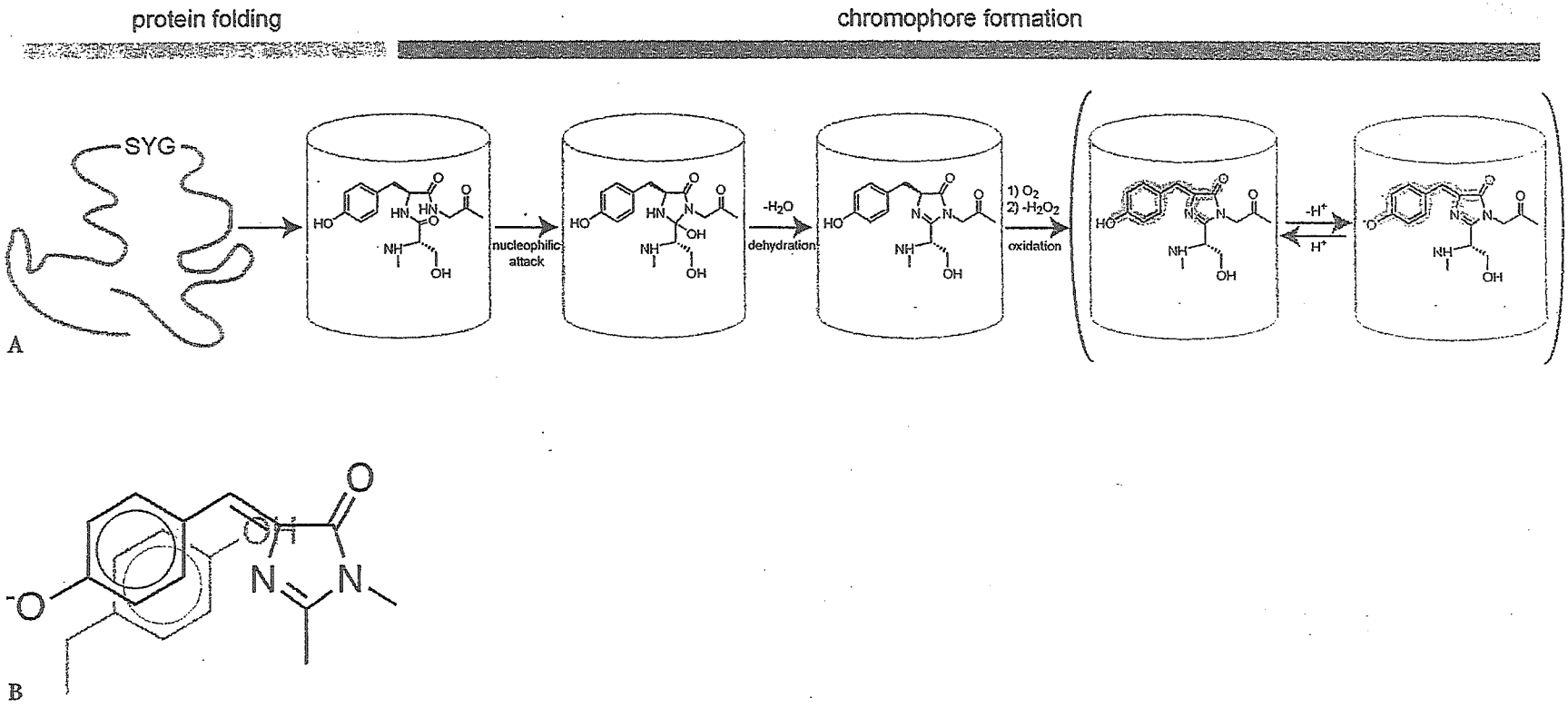

Fig. 1 A Diagram representing *Aequorea* GFP folding and chromophore formation. The β-can structure represents the native conformation of the protein, while the denatured form is depicted as an irregular chain. π-conjugation for visible-light absorption is indicated in *gray*. B Chromophore structure of YFP. Reprinted with permission from Miyawaki et al., Curr. Opin. Chem. Biol. 7, 558 (2003). Copyright © 2003 Elsevier

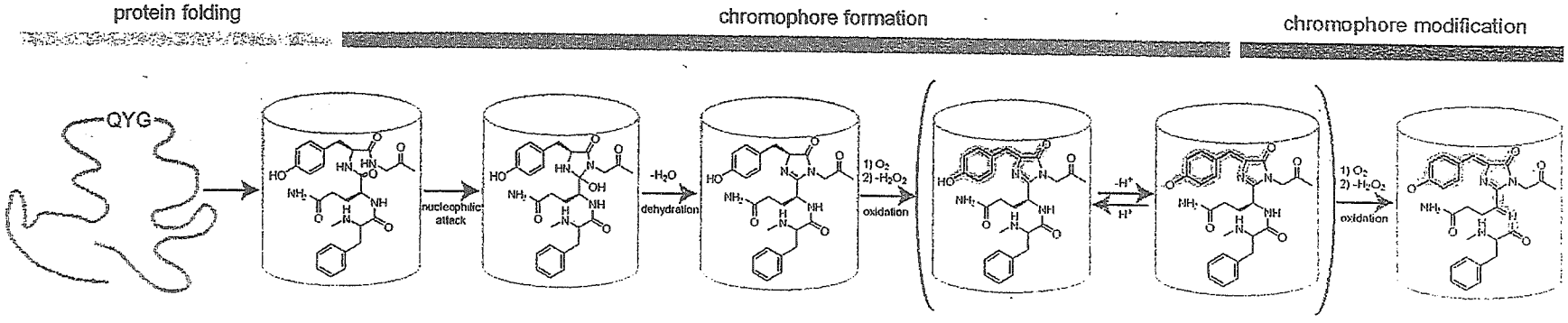

Fig. 2 Schematic of folding, chromophore formation, and chromophore modification of DsRed. The β-can structure represents the native conformation of the protein, while the denatured form is shown as an irregular chain. It is not known at which step oligomerization occurs. π-conjugation for visible-light absorption is indicated in *gray*. Reprinted with permission from Miyawaki et al., Curr. Opin. Chem. Biol. 7, 560 (2003). Copyright © 2003 Elsevier

mophore identical to GFP to generate its green intermediate [6]. Subsequently, the Cα-Nα bond of Gln^{66} oxidizes as the protein matures to become red (Fig. 2). The following section describes recent improvements in both YFP and DsRed maturation speed and/or fluorescence efficiency.

1.2 Improvements in Maturation of YFP

Two bright versions of YFP, Venus [7] and citrine [8], have recently been developed that mature quickly and efficiently, allowing for immediate detection of fluorescence signals after gene-introduction. Venus has a new mutation, F46L, and four common folding mutations, F64L, M153T, V163A, and S175G. The superiority of Venus to EYFP in terms of maturation is best observed following the re-naturation/re-oxidation profile of each protein. The chromophores of urea-denatured Venus and EYFP were reduced with 5 mmol/l dithionite [9], and re-naturation and re-oxidation were initiated by dilution at 37 °C (Fig. 3). Since oxidation is the rate-limiting step, the observed overall rate of fluorescence recovery under these circumstances should represent the rate of oxidation of the cyclized chromophore. The speed and yield of the re-naturation from denatured/reduced protein was significantly improved in Venus, which contains the F46L mutation (Fig. 3). To examine whether this mutation facilitates the maturation of any other *Aequorea* GFP variants, we introduced F46L into enhanced versions of blue, cyan, and green fluorescent proteins (Clontech). None of these mutants, however, displayed enhanced maturation

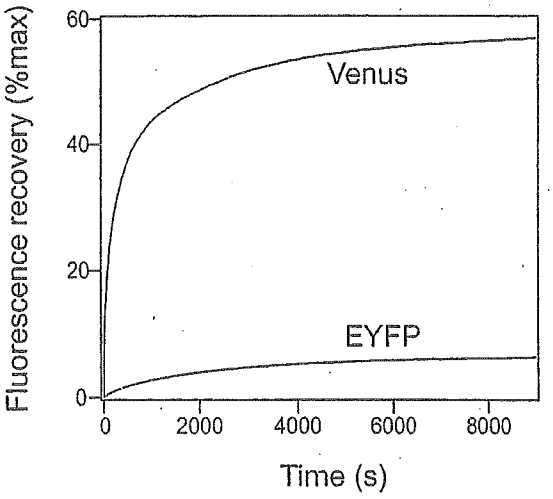

Fig. 3 Time course of fluorescence recovery of Venus and EYFP from their denatured/reduced state. For preparation of denatured/reduced protein samples, 5 mmol/l dithionite was added to denaturation buffer (8 mol/l urea and 1 mmol/l DTT). Recovery of fluorescence was initiated by a 100-fold dilution into re-naturation buffer (35 mmol/l KCl, 2 mmol/l $MgCl_2$, 50 mmol/l tris pH 7.5, 1 mmol/l DTT) at 37 °C. The emission at 530 nm was monitored by excitation at 515 nm. Reprinted with permission from Miyawaki et al., Curr. Opin. Chem. Biol. 7, 559 (2003). Copyright © 2003 Elsevier

[7]. On the other hand, the citrine version of YFP possesses a single mutation, Q69M [8].

Citrine and Venus have two main features in common. First, they both are yellow variants of GFP which have mutations, Q69M and F46L, respectively, which are specific to YFP. Second, they have similar backgrounds, arising from concerted efforts to improve the genetically encoded Ca^{2+} indicators, camgaroo [10] and pericam [11], respectively. As will be discussed below, camgaroo is a YFP variant into which calmodulin (CaM) has been inserted in place of Tyr145 of YFP; pericam was created by inserting a circularly-permuted YFP (cpYFP) between CaM and M13 (a CaM-target peptide). Since the original versions of camgaroo and pericam showed poor expression at 37 °C, their cDNAs were randomly mutated and screened in *E. coli* for maximal fluorescence. The Q69M and F46L mutations were found to be the most beneficial for improving the brightness of camgaroo and pericam, respectively, and these mutations were subsequently transferred into YFP to generate citrine and Venus. To engineer brighter GFP variants, therefore, it appears that the most efficient method may be to choose dimmer variants as parental constructs for mutagenesis. There is no guarantee, however, that the mutations discovered through this process will be effective for improving current bright variants. Though the crystal structures of citrine [8] and Venus [12] have been determined at 2.2 Å resolution, it is still unclear how the Q69M and F46L mutations act to accelerate the rate of oxidation of the Cα-Cβ bond of Tyr66.

The improved brightness should also be discussed in terms of the extent of quenching of the fluorophore by environmental factors. Among *Aequorea* GFP variants, YFPs are relatively acid sensitive, and uniquely quenched by halide ions, including chloride (Cl^-). Proton (H^+) and Cl^- synergistically affect the charge state of the chromophore of YFP, thereby suppressing its fluorescence. Citrine and Venus show increased resistance to both H^+ and Cl^- [7, 8].

1.3 Improvements in Maturation of DsRed

Compared with *Aequorea* GFP, DsRed has three unique features. First, the maturation process of DsRed includes a chromophore modification step which is responsible for changing its emission color from green to red (Fig. 2). Second, DsRed matures more efficiently at 37 °C than at room temperature, in contrast to *Aequorea* GFP, which folds preferentially at lower temperatures [13]. This may be directly traced to the differing water temperatures of the source organisms' habitats; *Aequorea victoria* is found in the Pacific Northwest, while *Discosoma* is native to the Indo-Pacific Ocean. Third, like many other Anthozoan GFP-like proteins, DsRed forms a tight tetrameric complex [14]. This tetrameric complex formation has been shown to be required for the development of red fluorescence [15], but it has not yet been determined which maturation step requires this process. Such tight oligomerization has probably evolved to maximize thermotolerance under conditions of intense tropical

sunlight. Very recently, Campbell et al. reported the successful engineering of monomeric RFP (mRFP1) from DsRed [16]. Their approach employed site-directed mutagenesis to break the tetrameric structure followed by random mutagenesis to rescue the original red fluorescence. The success of this work offers great hope regarding the conversion of other oligomeric fluorescent proteins into monomers. Another solution to the problem of RFP oligomerization reported by Campbell et al. [16] was to concatenate two dimer forming subunits of a mutant of DsRed with a spacer, which facilitates their dimer interactions through intramolecular contacts.

Incomplete chromophore modification of DsRed gives rise to residual green fluorescence, prohibiting the combined use of this molecule with green-emitting FPs in dual-color labeling experiments. The commercially available DsRed2 (Clontech) demonstrates only modest improvements in chromophore modification, but more recently, the release of engineered variants of DsRed known as T1 [17] and E57 [18] have enabled researchers to overcome the problems associated with slow and incomplete modification. Comparative analysis of these mutants in the context of the crystal structure of DsRed suggests available space around the chromophore is crucial for fast and complete modification [18]. Conversely, a long-lived green state can be advantageous for analysis of the history of gene expression in a cell. A new mutant of DsRed, E5, is particularly useful as it changes color from green to red in a predictable time course [19]. This feature makes it possible to use the ratio of green to red emission as an estimate of the time elapsed after initiation of reporter gene expression. Therefore, E5 functions as a fluorescent timer that yields temporal and spatial information regarding target promoter activity.

2
Engineering for Photoactivation and Photoconversion

2.1
Photoactivatable GFP

In the past two years, three new fluorescent protein variants have been generated that allow the selective activation or color conversion of fluorescent signal after specific illumination. The first variant, PA-GFP (photoactivatable GFP) [20] is based on wild-type *Aequorea* GFP, which has a bimodal absorption or excitation spectrum with two peak maxima, at 395 and 475 nm, corresponding to the protonated and the deprotonated states of the chromophore, respectively. When excited at 475 nm, wild-type *Aequorea* GFP emits maximal fluorescence at 503 nm, while excitation at 395 nm yields a maximum at 508 nm [2]. The latter large Stokes shift results from excited state deprotonation of the chromophore, as phenols become greatly more acidic in their excited states. Thus, excitation of the protonated chromophores gives emission at greater than 500 nm, similar to the direct excitation of the deprotonated chromophore.

Although the proton transfer is eventually reversible, the protonated chromophore is irreversibly isomerized to the deprotonated form upon intense illumination at 395 nm. The light transforms the species with the protonated chromophore, which absorbs at 395 nm, into the deprotonated species, which absorbs at 475 nm [2]. A recent cryospectroscopy, mass spectroscopy, and crystallography study on the photoconverted product showed that this photoconversion is a one-photon process paralleled by decarboxylation of a glutamic acid residue at position 222 [21]. Patterson and Lippincott-Schwartz found that substitution of histidine for threonine at position 203 was effective in decreasing the initial absorbance at 475 nm [20]. The resulting mutant, PA-GFP, exhibits up to a 100-fold increase in green fluorescence excitation at 488 nm when illuminated with 413-nm light.

2.2 Kaede

Around the same time, a green-emitting FP cloned from the stony coral *Trachyphyllia geoffroyi* was serendipitously discovered by Ando et al. to be useful as an optical cell marker [22]. The discovery occurred when the researchers accidentally left a test tube of the protein on a lab bench near a window, and found after a while that it had turned red. The naturally-engineered FP was named Kaede, the Japanese word for "maple leaf". Kaede contains a tripeptide, His^{62}-Tyr^{63}-Gly^{64}, which acts as a green chromophore that can be photoconverted to red. In its green state, it has two absorption peaks at 380 and 508 nm, corresponding to the neutral and ionized form, respectively. The neutral form of this molecule is highly sensitive to irradiation with UV or violet light (350–400 nm), which produce excitation and photoconversion. Interestingly, it has been observed that the photoconverted Kaede dissociates into 19- and 10-kDa fragments on SDS/PAGE. The structural basis for the green-to-red photoconversion has recently been presented [23]. As in *Aequorea* GFP, a chromophore, 4-(*p*-hydroxybenzylidene)-5-imidazolinone, derived from the

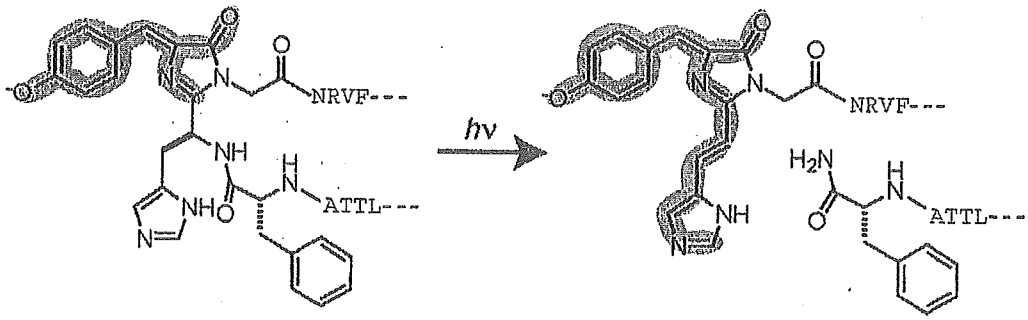

Fig. 4 Scheme for the formation and photo-induced extension of the chromophore of Kaede. Structures derived from Phe^{61}, His^{62}, Tyr^{63}, and Gly^{64} are drawn, and the neighboring amino acids (single-letter code) are added. π-conjugation for visible-light absorption is indicated in *gray*

tripeptide mediates green fluorescence in Kaede. UV irradiation causes an unconventional cleavage within Kaede protein between the amide nitrogen and the α carbon (Cα) at His^{62} via a formal β-elimination reaction, which requires the whole, intact protein for its catalysis. The subsequent formation of a double bond between His^{62}-Cα and -Cβ extends the π-conjugation to the imidazole ring of His^{62}, creating a new red-emitting chromophore, 2-[(1*E*)-2-(5-imidazolyl)ethenyl]-4-(*p*-hydroxybenzylidene)-5-imidazolinone (Fig. 4).

2.3 Kindling Fluorescent Protein

Lastly, Chudakov et al. showed that asCP, a unique GFP-like non-fluorescent chromoprotein from the sea anemome *Anemonia sulcata*, becomes fluorescent ("kindles") upon green light irradiation, with maximal emission at 595 nm [24]. Interestingly, asCP also has a histidine residue at position 203 (numbering in accordance with GFP alignment). More recently, they have generated a practically-useful mutant of asCP (designated KFP1) by replacing the alanine at position 148 with glycine [25]. KFP1 displays a roughly 30-fold increase in red fluorescence following excitation at 532 nm. This process is reversible, and can be controlled by both the light intensity level and the total light dose.

2.4 Histidine for Photochemical Reactions

It should be noted that all three of these variants carry histidine residues within or near the chromophore, suggesting the active involvement of histidine in photochemical reactions. Histidine, however, appears to play different roles depending on whether it is situated outside the chromophore at position 203 (PA-GFP and KFP1) or within the chromophore (Kaede). Studies by Ando et al. [22] and Chudakov et al. [24] have addressed the molecular mechanisms behind color variation occurring within individual coral animals. When exposed to sunlight, the tentacles and disk of the coral animals turn a shade of red in proportion to the degree of photoconversion. Then they revert to their previous colors as newly-synthesized proteins are added. Mechanisms such as this may be responsible for the great variety of color observed in coral reefs.

3 Engineering for Disruption of Oligomerization

Whether a fluorescent protein tends to form oligomers is an important consideration, as such interactions can interfere with the function of the host protein to which it is fused. Unfortunately, all of the *Anthozoan* GFP-like proteins

characterized so far form obligate oligomers [26]. While oligomerization does not prevent their use for reporting gene expression or marking cells, it does preclude their use in fusion protein applications. Similarly, fusion of DsRed, which normally forms a tetramer, to host proteins often disrupts their normal behavior, although there are some exceptions. As the monomeric RFP (mRFP1) matures ten times faster than its parental protein, it exhibits similar brightness to DsRed in living cells despite its lower molar extinction coefficient, fluorescence quantum yield and photostability. Because it is monomeric, mRFP1 has enabled red-fluorescence labelings that were not possible before with DsRed. Also, the excitation and emission maxima of mRFP1 are 584 and 607 nm, respectively, which gives good spectral separation from other FP signals. This work provides hope that other oligomeric FPs might also be converted into monomers. Indeed, the far-red variant HcRed1, made from a parent chromoprotein that seems to form obligate tetramers, has also been engineered to form dimers [27]. Similarly, a green-emitting FP recently cloned from *Galaxeidae* coral, Azami Green (AG) has been engineered to monomers (mAG) [28]. The anemone fluorescent protein epFP611 can function as a monomer, but only at low concentrations in the presence of detergent [29].

A further problem is the potential aggregation of fluorescent proteins, which impedes any cellular application and leads to cellular toxicity. Although the molecular mechanisms of FP aggregation remain unclear, there are two possible explanations. First, aggregation may be due to electrostatic or hydrophobic interactions between FPs. The possible contribution made by electrostatic interactions has been supported by recent work in which non-aggregating mutants were successfully generated by removing basic residues located near the amino termini of several fluorescent proteins [30], including DsRed. So, it may also be possible to make non-aggregating mutants by removing hydrophobic side chains on the surface of oligomeric complexes. It should be noted that *Renilla* GFP becomes soluble as a result of its dimerization; a hydrophobic patch becomes hidden at the dimerization interface and allows the surface of the dimer to become hydrophilic. The second possibility is that aggregation may follow FP oligomerization. Thus, the problem might be made worse still if host proteins are also oligomeric, as fusion to FPs might result in crosslinking into massive aggregates. Indeed, DsRed tends to produce more serious aggregation when fused to a host protein although, in an exception to this trend, fusion of DsRed to protein kinase C-γ retains the dynamic redistribution of the enzyme after stimulation. Overall, this aggregation problem would most easily be solved by using monomeric FPs.

Aequorea GFP has a propensity to weakly dimerize (Kd=0.1–0.3 mmol/l) [2]. Non-dimerizing CFP and YFP (mCFP and mYFP) have been constructed and utilized successfully in FRET experiments to determine how lipid-modified proteins assemble in the microdomains of the plasma membrane [31].